PCCP

Electron and energy transfer in a porphyrin-oxoporphyrinogen-fullerene triad, ZnP-OxP-C_{60}

Journal:	*Physical Chemistry Chemical Physics*
Manuscript ID	CP-COM-05-2020-002696.R2
Article Type:	Paper
Date Submitted by the Author:	16-Jun-2020
Complete List of Authors:	Chahal, Mandeep K.; National Institute for Materials Science, International Center for Materials Nanoarchitectonics Gobeze, Habtom; University of North Texas, Chemistry Webre, Whitney; University of North Texas, Department of Chemistry Karr, Paul; Wayne State College, Department of Physical Sciences and Mathematics Payne, Daniel; National Institute for Materials Science, ICYS Ariga, Katsuhiko; National Institute for Materials Science, World Premier International (WPI) Research Center for Materials Nanoarchitectonics (MANA) D'Souza, Francis; University of North Texas, Chemistry Hill, Jonathan; National Institute for Materials Science, International Center for Materials Nanoarchitectonics

ARTICLE

Electron and energy transfer in a porphyrin-oxoporphyrinogen-fullerene triad, ZnP-OxP-C_{60}†

Received 00th January 20xx,
Accepted 00th January 20xx

DOI: 10.1039/x0xx00000x

Mandeep K. Chahal,[a‡] Habtom B. Gobeze,[b‡] Whitney A. Webre,[b] Paul A. Karr,[c] Daniel T. Payne,[d] Katsuhiko Ariga,[ae] Francis D'Souza*[b] and Jonathan P. Hill*[a]

A multichromophoric triad, **ZnP-OxP-C_{60}** containing porphyrin (**ZnTPP** hereafter **ZnP**), oxoporphyrinogen (**OxP**) and fullerene (C_{60}) has been synthesized to probe the intramolecular dynamics of its electron and energy transfer in relation to the presence of the closely linked electron deficient **OxP-C_{60}** 'special pair', constructed as a mimic of the naturally occurring photosynthetic antenna-reaction center. The DFT optimized structure of the triad reveals the relative spatial remoteness of the **ZnP** entity with proximal **OxP/C_{60}** entities. Free-energetics of different energy and electron transfer events were estimated using spectral, computational and electrochemical studies, according to Rehm-Weller approach. Femtosecond transient absorption spectral studies revealed energy transfer from ^{1}**ZnP*** to **OxP** to yield **ZnP-^{1}OxP*-C_{60}**, and electron tranfer to yield **ZnP$^{\cdot+}$-OxP-$C_{60}^{\cdot-}$** and/or **ZnP-OxP$^{\cdot+}$-$C_{60}^{\cdot-}$** charge seperated states. That is, the **ZnP** entity in the triad operates as both antenna and electron donor to generate relatively long-lived charge separated states thus mimicking the early photoevents of natural photosynthesis. Abstract text goes here. The abstract should be a single paragraph that summarises the content of the article

Introduction

Oligochromophoric molecules have been studied intensively as models of naturally-occurring photosynthetic pigments in order to better understand interchromophore interactions and ultimately to assist in the design of light harvesting molecular systems.[1,2] Naturally-occurring systems have evolved to contain photo- and electrochemical gradients that sequester, transfer and convert incident photons to chemical energy.[3] These processes respectively involve absorption, energy transfer and charge separation reactions whose potential is captured and fixed as chemical bonds.[3] Different features have been reproduced in synthetic molecular systems,[4,5] which can be considered biomimetic,[6] usually involving chromophore compounds quite similar to those of the natural systems (i.e. tetrapyrroles[7]), or by using man-made pigments where factors such as stability under irradiation or wavelength of light absorbance can be controlled.[8,9] These often large molecular constructs with molecular weights similar to those of small proteins have properties that can be influenced by external factors such as solvent polarity[10] or the presence of guest species, so-called cofactors.[11]

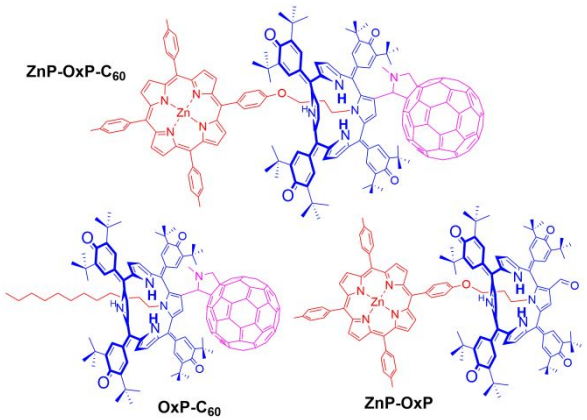

Fig. 1. Structures of the triad., **ZnP-OxP-C_{60}** and the diads **OxP-C_{60}** and **ZnP-OxP** studied here.

The assembly of an oligochromophoric system can be achieved by supramolecular methods[12] or can be based on covalent methods.[13] The advantages of the latter include improved chemical stability and the lack of consideration for weaker intermolecular interactions leading to disordered structures. Disadvantages include possible aggregative processes and the existence of multiple conformations of the same molecule which would obstruct interpretation of spectroscopic data (although any large molecular system including supramolecular manifolds suffer from this). For this work, the covalent route to the preparation of a multimodule organic chromophore for its study as a model light harvesting system was selected. Molecular systems designed to mimic photosynthetic

[a.] *International Centre for Materials Nanoarchitectonics (WPI-MANA), National Institute for Materials Science (NIMS), Namiki 1-1, Tsukuba, Ibaraki, 305-0044, Japan. E-mail: Jonathan.Hill@nims.go.jp*
[b.] *Department of Chemistry, University of North Texas, 1155 Union Circle, #305070, Denton, TX 76203-5017, United States; E-mail: Francis.dsouza@unt.edu.*
[c.] *Department of Physical Sciences and Mathematics, Wayne State College, 111 Main Street, Wayne, Nebraska, 68787, USA.*
[d.] *International Centre for Young Scientists (ICYS), National Institute for Materials Science (NIMS), Namiki 1-1, Tsukuba, Ibaraki, 305-0044, Japan.*
[e.] *Department of Advanced Materials Science, Graduate School of Frontier Sciences, The University of Tokyo, 5-1-5 Kashiwanoha, Kashiwa, Chiba 277-8561, Japan.*
‡These authors contributed equally.
†Electronic Supplementary Information (ESI) available: [details of any supplementary information available should be included here]. See DOI: 10.1039/x0xx00000x

processes are often composed of excessively large multichromophore systems whose purification and characterization are inconvenient. This makes their application in any potential devices inconvenient. For this reason, we have designed and synthesized a family of molecules to probe the possibility of preparing manageable small molecule microcosms of the large chromophore assemblies responsible for photosynthetic processes.

In previous work, we have noted that the **OxP** chromophore can operate as electron donor or acceptor.[14,15] This fact, coupled with its synthetic flexibility, has permitted the synthesis of the compounds shown in Fig. 1. Incorporation of the **OxP** unit has the additional effect of substantially increasing the solubilities of its compounds in common solvents partly due to the presence of eight solubilizing *t*-butyl groups but also because the connectivity at calix[4]pyrrole N-atoms reduces molecular rigidity in these systems, disfavouring aggregation. The triad **ZnP-OxP-C_{60}**, whose energetic and electronic interplay under irradiation are the subject of this work, was studied alongside **OxP-C_{60}** and **ZnP-OxP** essential control diads prepared to demonstrate the relative properties. Synthesis of the triad is allowed by regioselectivity of N-alkylation on **OxP-CHO**.[16]

Here we report the properties of oligochromophore structures containing the commonly used **ZnP** and **C_{60}** chromophores[17,18] attached to the highly coloured and π-conjugated oxoporphyrinogen, **OxP**.[19] We show that the structure of the **ZnP-OxP-C_{60}** triad confers specific roles of the components as energy harvesting moiety (**ZnP**) whose action stimulates the formation of charge separated (CS) state between **OxP** and **C_{60}**. Thus, **ZnP-OxP-C_{60}** can be seen as a small molecule analogue of photosynthetic systems since energy harvested by the single porphyrin group leads to formation of the CS state. The **OxP** unit is revealed as a multitasking chromophore in these molecules described since it undergoes photo-induced oxidation as well as being capable of light absorption in the visible range.

ZnP-OxP-C_{60} was synthesized from **OxP-CHO**[16] by first N-alkylated at pyrrolic NH group yielding mono-N-porphyrinyl-**OxP-CHO** followed by Prato reaction[20] yielding the covalently linked donor-acceptor multichromophore. In more detail (see also Scheme S1), mono-alkylation of **OxP-CHO** was achieved by refluxing it with 3 equiv. of [5-(4-(3-bromopropoxy)phenyl)]-10,15,20-tris(4-methyl phenyl)porphyrinato]zinc(II) in dry acetone for 24 hours in the presence of sodium carbonate. For **ZnP-OxP**, N-alkylation occurs regioselectively at N_{21}. Triad **ZnP-OxP-C_{60}** was then synthesized under Prato reaction conditions by refluxing the formylated precursor **ZnP-OxP**-(CHO) with fullerene and N-methylglycine in toluene for 12 hours. Purification of the compounds was performed using gel permeation chromatography on BioBeads SX-1 eluting with dichloromethane followed by preparative thin layer chromatography. Other compound prepared (using the same methods as mentioned above) as controls include (*n*-$C_{12}H_{25}$)-**OxP-C_{60}**, which lacked porphyrin.

Fig. 2 shows the absorption spectrum of the triad and control diads in *o*-dichlorobenzene (DCB). Bands due to **ZnP** occur at 426 (Soret), 550 and 590 nm (Q bands). For both **ZnP-OxP** dyad and **ZnP-OxP-C_{60}** triad, Q bands appear as shoulder peaks of the broad **OxP** absorption at 450-700 nm (**OxP** maximum at 518 nm). Absorbances due to **C_{60}** coincide with the strong bands due to **ZnP** and **OxP** entities of the triad. Excitation of the triad at the Soret band leads to very weak fluorescence at 600 and 650 nm assigned due to emission by **ZnP**. Further weak emission at 715 nm is assigned to **OxP**. The strong quenching of **ZnP** and appearance of the band due to **OxP** peak suggest the possibility of energy transfer in **ZnP-OxP-C_{60}**.[21]

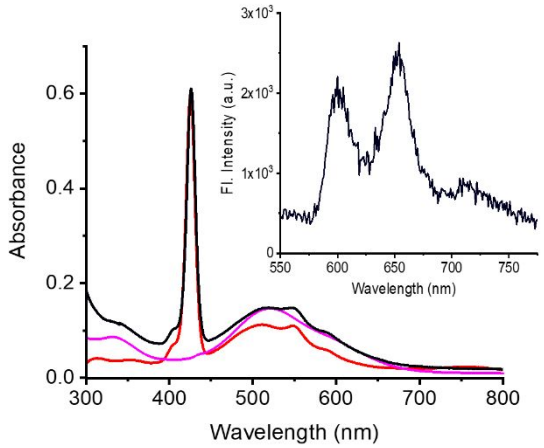

Fig. 2. Normalized (Soret) absorption spectra of **ZnP-OxP-CHO** dyad (red), **ZnP-OxP-C_{60}** (black) and **OxP-C_{60}** (magenta) in DCB. Inset shows fluorescence of **ZnP-OxP-C_{60}** (λ_{EX} = 426 nm, **ZnP**).

Next cyclic voltammetry of the triad and controls (used to deduce the sites of electron tranfer) were performed (Fig. 3). In the triad, the first oxidation at 0.85 V vs. Ag/AgCl is **ZnP** centered while the second at 1.16 V contains both **OxP** first oxidation and **ZnP** second oxidation processes. On the cathodic side, the first reduction at -0.62 V is **C_{60}** centered, the second at -0.85 V due to **OxP**, with the third process at -1.02 V being due to the second reduction of **C_{60}**. The fourth reduction at -1.37 V is due to the first reduction of **ZnP**.

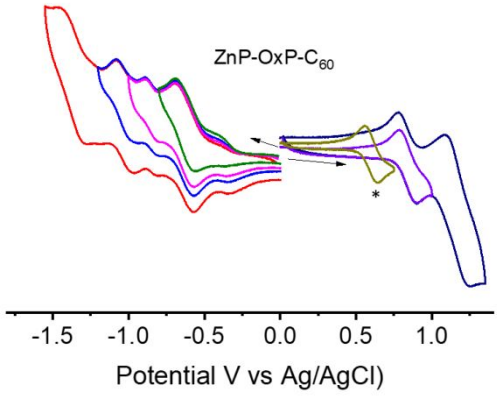

Fig. 3. Cyclic voltammograms (CV) of **ZnP-OxP-C_{60}** in DCB containing 0.1 M (TBA)ClO_4. Reversibility of each redox process is shown by changing the direction of potential scan immediately after each wave with each highlighted in a different colour (1st reduction: green, 2nd reduction: pink, 3rd reduction: blue, 4th reduction: red, 1st oxidation: purple, 2nd oxidation dark blue). Voltammogram with asterisk represents oxidation of ferrocene used as an internal standard.

The geometry and electronic structure of the triad was deduced by optimizing the **ZnP-OxP-C_{60}** structure at the B3LYP/6-311G(d,p) level.[22] In the optimized structure, the **OxP** entity is positioned in between the **ZnP** and **C_{60}** entities (Fig. 4). The nonplanar saddle-like structure of **OxP** allows this geometry with a single pyrrole ring

carrying both **ZnP** and C_{60}. This also substantially separates **ZnP** and C_{60} minimizing intramolecular effects due to the connectivity and the sterically bulky **OxP** unit. Centre-to-centre distances are C_{60}/**ZnP** (19.7 Å), **OxP**/C_{60} (9.8 Å), and **OxP**/**ZnP** (14.7 Å). It is important to note the spatially distant **ZnP** and closely associated **OxP**/C_{60} entities within the triad. In accordance with electrochemical results, molecular orbitals were found at HOMO-2 on **OxP**, HOMO on **ZnP** and LUMO on C_{60}. The molecular electrostatic potential map of **ZnP-OxP-**C_{60} also revealed electron rich and deficient sites of the triad.

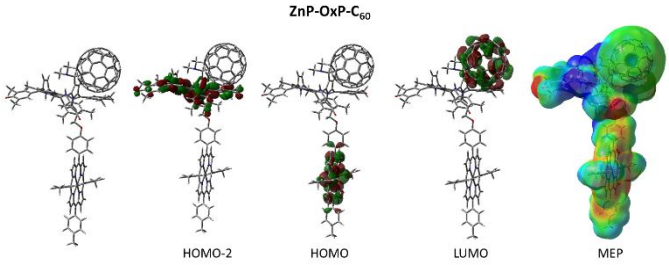

Fig. 4. B3LYP/6-311G(d,p) optimized structure, HOMO-2, HOMO, LUMO and molecular electrostatic potential map (MEP) for the **ZnP-OxP-**C_{60} triad.

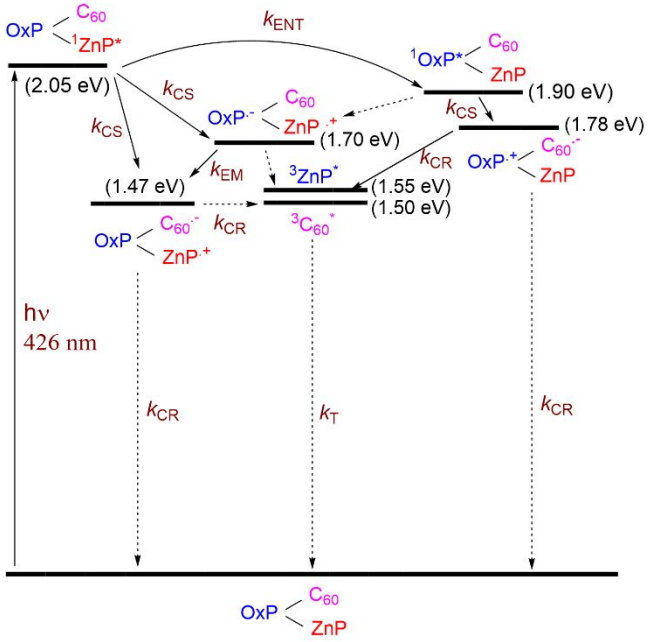

Fig. 5. Energy level diagram depicting different photoinduced energy and electron transfer events in the studied **ZnP-OxP-**C_{60} triad. Abbreviations: ENT = energy transfer, CS = charge separation, CR = charge recombination, T = triplet state, EM = electron migration, solid arrow = major path, dashed arrow = minor path.

An energy level diagram for different photochemical events upon excitation of **ZnP** at 426 nm (Soret band), where interference from other entities is minimal, was constructed (Fig. 5). Energies of the different states were calculated according to the Rehm-Weller approach.[23,24] ^{1}**ZnP*** produced by excitation in the triad might undergo at least three photoinduced events, namely, energy transfer to **OxP** to produce **ZnP-**^{1}**OxP*-**C_{60} or oxidative electron transfer to produce **ZnP**$^{\cdot+}$**-OxP-**$C_{60}^{\cdot-}$ and/or **ZnP**$^{\cdot+}$**-OxP**$^{\cdot-}$**-**C_{60} CS states. Furthermore, the energetically high lying **ZnP**$^{\cdot+}$**-OxP**$^{\cdot-}$**-**C_{60} state could undergo electron migration (EM) to produce the **ZnP**$^{\cdot+}$**-OxP-**$C_{60}^{\cdot-}$ CS state. The large separation between radical cation and radical anion in the **ZnP**$^{\cdot+}$**-OxP-**$C_{60}^{\cdot-}$ CS state (formed directly or by EM) implies the formation of a long-lived charge separated state. In addition, the **ZnP-**^{1}**OxP*-**C_{60} state could undergo oxidative electron transfer to yield **ZnP-OxP**$^{\cdot+}$**-**$C_{60}^{\cdot-}$ CS state. Interestingly, **ZnP**$^{\cdot+}$**-OxP**$^{\cdot-}$**-**C_{60} and **ZnP-OxP**$^{\cdot+}$**-**$C_{60}^{\cdot-}$ CS states are higher in energy than both ^{3}**ZnP*** and ^{3}C_{60}* so that intramolecular processes could also lead to population of one of these triplet states.

For assignment of peaks, from spectroelectrochemical studies and previous work, the peak due to **ZnP**$^{\cdot+}$ is in the 620-700 nm range,[25] while that due to $C_{60}^{\cdot-}$ lies in the 1020 nm range,[26] as is well-know. To characterize **OxP**$^{\cdot+}$, pristine **OxP** was treated using the one-electron oxidant nitrosonium tetrafluoroborate, as shown in Fig. S1. The emerging new peak at 720 nm corresonding to the formation of **OxP**$^{\cdot+}$ was observed.

Femtosecond transient absorption (fs-TA) spectral studies on both the control diads and the triad were performed to probe the photochemical events predicted by Fig. 5. Fig. 6a shows fs-TA spectra at the indicated delay times of **OxP-**C_{60} diad at λ_{ex} = 550 nm corresponding largely to **OxP**. The instantaneously formed ^{1}**OxP*** leads to ground state bleaching (GSB) at 520 nm, and excited state absorption (ESA) at 700 and 1005 nm. Recovery and decay of GSB and ESA peaks is accompanied by new peaks at 720 nm corresponding to **OxP**$^{\cdot+}$ and at 1000 nm corresponding to $C_{60}^{\cdot-}$ confirming the formation of **OxP**$^{\cdot+}$**-**$C_{60}^{\cdot-}$ CS state. A new peak corresponding to ^{3}C_{60}* emerges at 700 nm[27] with decay of the CS signals indicating population of this state. From global analysis, decay associated spectra (DAS) were generated containing three components in the visible region and four components in the near-IR region. The first one with a time constant of 1.5 ps (not visible in the visible DAS) is attributed to a higher excited state species and vibrational relaxation **OxP**. The DAS at 21/27 ps (from visible/near-IR DAS analysis) is characteristic of ^{1}**OxP*** based on independent measurements. The third DAS at 216/230 ps contains a well-developed peak in the 720 nm range corresponding to **OxP**$^{\cdot+}$ and at 992 nm due to $C_{60}^{\cdot-}$ of the CS state. The fourth component with infinity time constant (> 3 ns) leads to a broad peak in the 700 nm range attributed to ^{3}C_{60}*.[27]

ZnP-OxP dyad was then investigated at a pumping wavelength of 426 nm mainly exciting the **ZnP** entity (Fig. 6b). Instantaneously formed ^{1}**ZnP*** exhibits ESA at 464 nm and GSB at 550 nm and stimulated emission (SE) at 690 nm. The decay/recovery of these peaks was accompanied by a new GSB at 514 nm and ESA peak at 700 nm corresponding to ^{1}**OxP***, indicating occurrence of energy transfer in this diad. DAS from global analysis revealed five components in the visible and four components in the near-IR region. DAS at 0.8 ps in the visible region (not shown) was characteristic of ^{1}**ZnP*** while the 3.9/6.2 and 64.3/49.2 ps were almost mirror image signals are attributed to growth and decay of ^{1}**OxP***. The fourth component at 762/833 ps is attributed to the CS state, **ZnP**$^{\cdot+}$**-OxP**$^{\cdot-}$ since the DAS spectrum contains a peak characteristic of **ZnP**$^{\cdot+}$ at 640 nm. The last DAS with infinite time constant can be attributed to ^{3}**ZnP*** as it revealed characteristic signals of this excited state.[28]

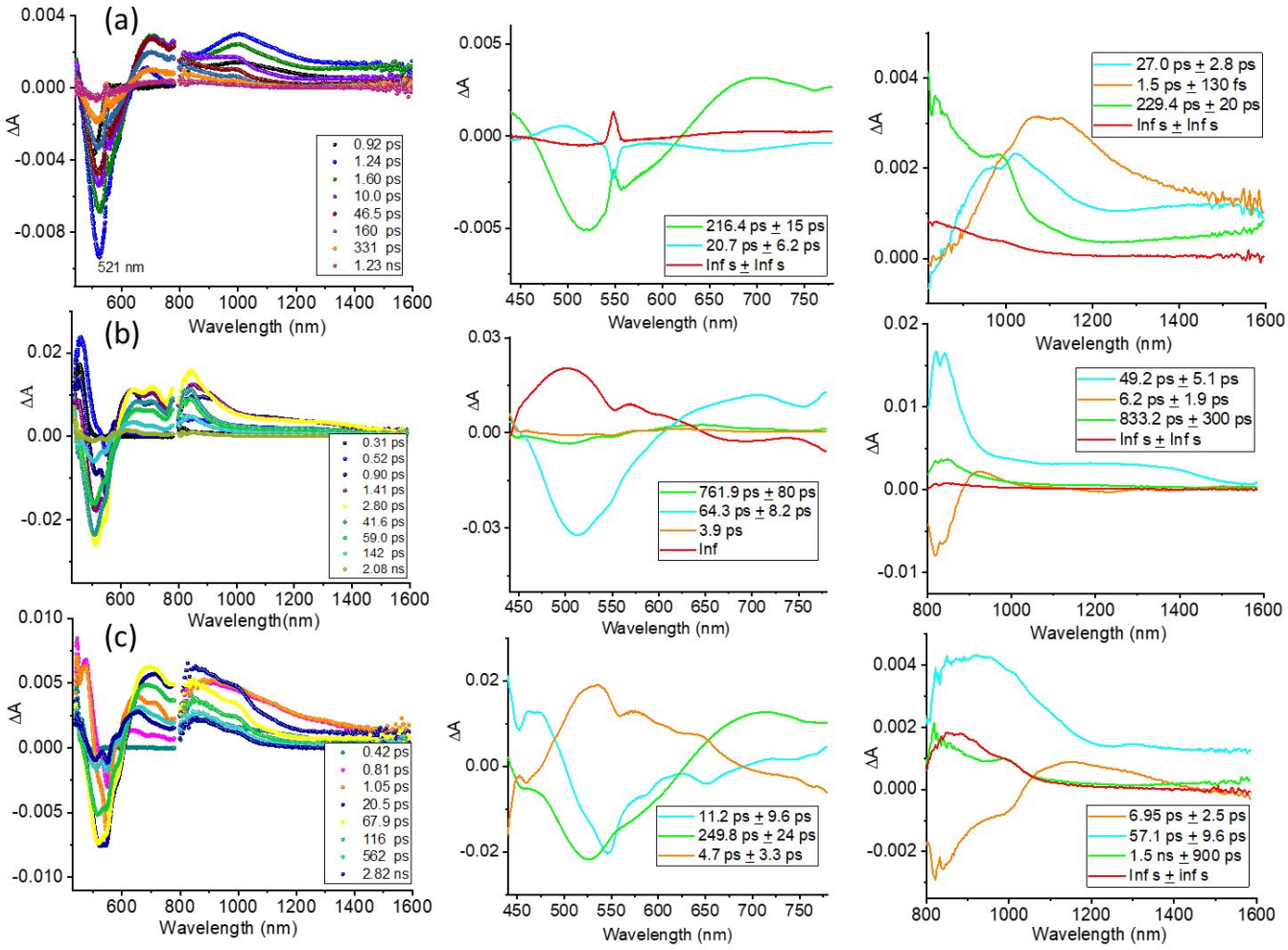

Fig. 6. Fs-TA spectra at the indicated delay times of (a) **OxP-C_{60}** (λ_{ex} = 550 nm), (b) **ZnP-OxP-CHO** (λ_{ex} = 426 nm), and (c) **ZnP-OxP-C_{60}** triad (λ_{ex} = 426 nm) in deaerated DCB. Decay associated spectra from global analysis are shown in the panels at centre (visible) and right (near-IR).

Finally, fs-TA spectra of the triad **ZnP-OxP-C_{60}** are shown in Fig. 6c for λ_{ex} = 426 nm. Instantaneously formed ^{1}ZnTPP* is indicated by ESA peak at 464, GSB at 550 and SE peak at 590 nm. However, fast relaxation/recovery of these peaks was accompanied by a GSB peak at 514 nm corresponding to **^{1}OxP*** formed by energy transfer. In the near-IR region, a peak characteristic of **$C_{60}^{\cdot-}$** at 1000 nm was also observed, suggesting formation of **ZnP$^{\cdot+}$-OxP-$C_{60}^{\cdot-}$** and/or **ZnP-OxP$^{\cdot+}$-$C_{60}^{\cdot-}$** CS states, as per Fig. 5. In the visible region, peaks at 720 nm and 640 nm respectively attributable to **OxP$^{\cdot+}$** and **ZnP$^{\cdot+}$** are present, although these peaks were strongly overlapped with ESA peaks due to **^{1}ZnP*** and **^{1}OxP*** in this range. The DAS spectra in the visible range revealed formation of **^{1}ZnP*** at 11.2 ps while the time constant for energy transfer product, **^{1}OxP*** was found at 250 ps (visible region DAS spectrum). In the near-IR DAS, of the four components, the 7 ps and 1.05 ns mirror image components contain the signature peak of **$C_{60}^{\cdot-}$** at 1000 nm. The 57 ps DAS contains singlet excited state features while the infinity DAS is due to triplet population. Importantly, the **OxP$^{\cdot+}$-$C_{60}^{\cdot-}$** CS state in the dyad, with a time constant of 0.83 ns, is shorter than that observed for the triad (1.5 ns), suggesting formation of the anticipated relatively long-lived **ZnP$^{\cdot+}$-OxP-$C_{60}^{\cdot-}$** state.

Conclusions

In summary, we have prepared a novel molecular triad containing the three chromophores **ZnP**, **OxP** and **C_{60}**. This has been made possible by regioselective N-alkylation of **OxP** available for **OxP-CHO**.[16] The optimized geometry of the triad revealed the relative spatial remoteness of the **ZnP** entity with proximal **OxP**/**C_{60}** entities. Energetics of different energy and electron transfer events were deduced using spectral and electrochemical studies. Fs-TA studies reveal energy transfer from **^{1}ZnP*** to **OxP** to yield **ZnP-^{1}OxP*-C_{60}**, and electron tranfer to yield **ZnP$^{\cdot+}$-OxP-$C_{60}^{\cdot-}$** and/or **ZnP-OxP$^{\cdot+}$-$C_{60}^{\cdot-}$** CS states. That is, the **ZnP** entity in the triad operates as both antenna and electron donor to generate relatively long-lived charge separated states, successfully mimicking the antenna-reaction centre events of natural photosynthesis. Notably, **OxP**, given its

synthetic flexibility and the solubility of its derivatives, turns out to be an excellent choice for the design and synthesis of multifunctional oligochromophore systems.

Experimental Section

General. Reagents and dehydrated solvents (in septum-sealed bottles) used for syntheses and spectroscopic measurements were obtained from Tokyo Kasei Chemical Co., Wako Chemical Co. or Aldrich Chemical Co. and were used without further purification. Preparative thin layer chromatography (PTLC) was performed using Analtech UNIPLATE™ PTLC silica plates (20 x 20 cm, 1500 microns). Gel permeation chromatography separations were performed with Bio-Beads™ S-X1. Electronic absorption spectra were measured using JASCO V-570 UV/Vis/NIR spectrophotometer, Princeton Applied Research (PAR) diode array rapid scanning spectrometer or a Shimadzu UV/Visible spectrophotometer. FTIR spectra were obtained from solid samples using a Thermo-Nicolet 760X FTIR spectrophotometer. ^{1}H NMR spectra were recorded on a JEOL AL300BX NMR spectrometer at 300 MHz, proton decoupled ^{13}C NMR were recorded at 75 MHz on a JEOL AL300BX NMR spectrometer at the stated temperatures. Data was processed on Delta version 5.0.5.1 and Always JNM-AL version 6.2. ^{1}H NMR chemical shifts (δ) are reported in ppm relative to TMS for $CDCl_3$ (δ 0.00) or the residual solvent peak for other solvents. ^{13}C NMR chemical shifts (δ) are reported in ppm relative to the solvent reported. Coupling constants (*J*) are expressed in Hertz (Hz), shift multiplicities are reported as singlet (s), doublet (d), triplet (t), quartet (q), double doublet (dd), multiplet (m) and broad singlet (bs). Matrix-assisted laser desorption time-of-flight mass spectra (MALDI-TOF-MS) spectra were measured using a Shimadzu-Kratos Axima CR+ spectrometer using dithranol as matrix. High resolution ESI-MS mass spectra were measured using a Thermo Scientific Q-Exactive Plus instrument with samples dissolved in dichloromethane (*c* = 1 mg/mL). The compounds [5-(4-(3-bromopropoxy)phenyl)]-10,15,20-tris(4-methylphenyl)porphyrinato]zinc(II)[29] and **OxP-CHO**[16] were prepared according to literature methods.

General Procedure for Prato Reaction.[20] Aldehyde (1 equiv.), N-methylglycine (4 equiv.) and fullerene, C_{60} (4 equiv.) were placed in a dry flask. Toluene was added and the reaction was heated at reflux for 12 hours under an atmosphere of nitrogen. The mixture was cooled to room temperature and the solvent was removed under reduced pressure. The residue was purified by using the gel permeation chromatography on BioBeads SX-1 eluting with dichloromethane. Further purification involved column chromatography (SiO_2) and preparative thin layer chromatography (PTLC) for some polyads (see synthetic procedures below).

2-Formyl-5,10,15,20-tetrakis(3,5-di-*tert*-butyl-4-oxo-cyclohexa-2,5-dienylidene)porphyrinogen, **OxP-CHO**. [T(DtBHP)P]Cu (1 g, 0.84 mmol, 1.0 equiv.) in dichloromethane (30 mL) was added to Vilsmeier reagent (prepared by adding phosphoryl chloride (8.12 g, 52.9 mmol, 63.0 equiv.) to DMF (5.96 g, 81.5 mmol, 97.0 equiv.) at 0 °C under nitrogen and stirred for 10 minutes). The reaction was heated at reflux for 18 hours. The resulting reaction mixture was cooled to 0 °C and conc. H_2SO_4 (☐ 6 mL) was added dropwise followed by stirring until complete demetallation had also occurred (organic layer turns colorless once demetallation is complete). The resulting solution was poured carefully into a mixture of aqueous NaOH solution (3M, 400 mL) and crushed ice then extracted with dichloromethane (3 x 100 mL). The organic fractions were combined, dried over anhydrous sodium sulfate and the solvents were removed under reduced pressure. The solid was redissolved in dichloromethane (100 mL) and tetrabutylammonium hydroxide solution (0.5 mL, 1.0 M in methanol) was added followed by stirring for 30 minutes. The resulting mixture was washed with water (200 mL), dried over anhydrous sodium sulfate and passed through a plug of silica (dichloromethane/acetone 9:1) to give after removal of solvents under reduced pressure **OxP-CHO** as a dark olive green solid (0.9 g, 93%). UV/Vis (CH_2Cl_2): 337 and 506 (λ_{max}) nm. FT-IR(KBr): *ν* = 3438.9 (w), 3179.0 (w), 2999.7 (w), 2952.1 (m), 2919.2 (m), 2862.9 (w), 1638.4 (m), 1605.3 (s), 1563.0 (s), 1485.1 (m), 1453.3 (s), 1388.0 (w), 1361.5 (s), 1340.7 (w), 1297.7 (m), 1264.1 (m), 1088.8 (m), 1027.6 (m), 997.2 (w), 939.5 (w), 929.5 (w), 885.9 (w), 834.6 (w), 819.1 (w), 802.0 (w) cm^{-1}; MALDI-TOF-MS (dithranol): calc'd for $[C_{77}H_{94}N_4O_5]^+$ = 1154.72; found: 1154.19 ($[M + 2H]^+$).

N_{21}-dodecyl-2-formyl-5,10,15,20-tetrakis(3,5-di-*tert*-butyl-4-oxo-cyclohexa-2,5-dienylidene)porphyrinogen, **OxP-DD-CHO**.

Alkylation of **OxP-CHO** was carried out according to a literature procedure.[19b] Dodecyl bromide (260 mg, 1.04 mmol, 4.0 equiv.) and sodium carbonate (1.1 g, 10.4 mmol, 40.0 equiv.) were added to **OxP-CHO** (300 mg, 0.26 mmol, 1.0 equiv.) in acetone (30 mL) then the mixture was heated at reflux for 12 hours. The reaction was monitored by using thin layer chromatography until the formation of mono-, di-alkylated products and full consumption of **OxP-CHO** was observed. The reaction solvent was removed under reduced pressure and the residue was partitioned between water (20 mL) and dichloromethane (30 mL), the organic phase was dried over anhydrous sodium sulfate, filtered and solvent was removed under reduced pressure. The residue was purified by column chromatography (SiO_2) eluting with dichloromethane. The first fraction eluted contained **OxP-DD_2-CHO**, which was isolated as a dark green solid (Yield: 194 mg, 50%) after evaporation of solvent and saved for use in future. Further elution with dichloromethane gave **OxP-DD-CHO** after evaporation of solvents under reduced pressure (Yield: 130 mg, 38%). UV/Vis (CH_2Cl_2): λ_{max} (ε, M^{-1} cm^{-1}) = 330 (27300), 504 (152600) nm. ^{1}H NMR (300 MHz): *δ* = 10.14 (s, 1H), 10.05 (s, 1H), 8.96 (s, 1H), 8.37 (s, 1H), 7.66-7.79 (m, 2H), 7.32-7.39 (m, 3H), 7.09-7.18 (m, 1H), 6.80-7.00 (m, 6H), 6.56 (s, 3H), 3.66-3.74 (m, 2H), 3.11-3.33 (m, 2H), 1.13-1.34 (m, 93H) ppm; ^{13}C NMR (76 MHz, $CDCl_3$): *δ* = 186.39, 186.19, 186.03, 150.30, 150.05, 149.77, 149.57, 149.10, 148.58, 148.41, 148.04, 135.40, 134.83, 134.74, 134.28, 134.17, 132.35, 131.64, 131.44, 131.29, 130.86, 130.59, 130.50, 130.16, 129.97, 129.78, 129.56, 126.13, 121.43, 121.23, 120.46, 119.74, 119.45, 119.12, 45.98, 36.22, 36.11, 35.96, 35.89, 35.81, 35.73, 32.17, 31.21, 30.50, 30.05, 29.91, 29.86, 29.57, 29.44, 26.68, 22.97, 18.79, 14.38 ppm; FT-IR(ATR): *ν* = 3435.3 (w), 2949.5 (m), 2920.3 (w), 2859.4 (w), 1704.1 (w), 1635.3 (w), 1589.7 (m), 1558.9 (w), 1485.9 (w),

1452.8 (m), 1404.8 (w), 1387.7 (w), 1358.6 (s), 1328.0 (w), 1297.4 (m), 1264.2 (m), 1202.4 (w), 1154.1 (w), 1087.8 (m), 1056.2 (w), 1027.2 (s), 997.6 (w), 960.1 (w), 942.4 (w), 929.3 (w), 883.4 (w), 838.5 (w), 801.2 (m), 771.8 (w), 743.8 (w), 711.3 (w), 627.3 (m), 530.4 (w), 518.0 (w) cm^{-1}; MALDI-TOF-MS (dithranol): calc'd for $[C_{89}H_{115}N_4O_5]^+$ = 1321 ([M + H]$^+$); HRMS (ESI-MS); calculated for $[C_{89}H_{115}N_4O_5]^+$ = 1319.8884, found: 1319.8867 ([M]$^+$).

OxP-C_{60} Dyad. The reaction was carried out according to General Procedure for Prato Reaction using **OxP-DD-CHO** (100 mg, 0.07 mmol, 1.0 equiv.), fullerene, C_{60} (218 mg, 0.30 mmol, 4.0 equiv.) and N-methylglycine (27 mg, 0.30 mmol, 4.0 equiv.) under reflux in toluene. The residue was purified by using gel permeation chromatography on BioBeads SX-1 eluting with dichloromethane. Further purification was by column chromatography (SiO_2) using dichloromethane as eluent. **OxP-C_{60}** was isolated as a dark green solid (Yield: 71 mg, 45%). UV/Vis (CH_2Cl_2): λ_{max} (ε, M^{-1} cm^{-1}) = 256 (144000), 330 (54800), 520 (113400) nm. ^{1}H NMR (300 MHz, $CDCl_3$): δ 8.12 (s, 1H), 7.94 (s, 1H), 7.75 (s, 1H), 7.59 (d, J = 2.2 Hz, 1H), 7.38-7.49 (m, 3H), 7.28 (d, J = 2.2 Hz, 1H), 7.13-7.24 (m, 3H), 6.60-6.86 (m, 7H), 4.87-4.90 (m, 2H), 4.08 (d, J = 9.5 Hz, 1H), 3.06-3.27 (m, 5H), 1.14-1.47 (m, 95H) ppm; ^{13}C NMR (76 MHz, $CDCl_3$): δ ppm; FT-IR(ATR): ν = 3410.7 (w), 2949.2 (m), 2920.0 (m), 2852.9 (m), 1724.8 (w), 1592.2 (s), 1544.2 (w), 1486.0 (m), 1450.8 (s), 1386.7 (w), 1358.7 (s), 1321.8 (w), 1295.5 (m), 1254.9 (m), 1203.9 (w), 1179.0 (w), 1086.2 (m), 1025.2 (s), 995.5 (w), 959.1 (w), 940.9 (w), 928.9 (w), 881.3 (w), 835.6 (w), 817.1 (w), 797.0 (m), 744.7 (w), 708.7 (w), 627.3 (w), 599.6 (w), 575.0 (w), 525.6 (s), 478.7 (w) cm^{-1}; MALDI-TOF-MS (dithranol): calculated for $[C_{151}H_{120}N_5O_4]^+$ = 2066 ([M - H]$^+$); HRMS (ESI-MS); calc'd for $[C_{151}H_{120}N_5O_4]^+$ = 2066.9335, found: 2066.9321 ([M – H]$^+$).

ZnP-OxP-C_{60} Triad. The reaction was carried out according to General Procedure for Prato Reaction using **ZnP-OxP-CHO (60 mg, 0.03 m**mol, 1 equiv.), fullerene C_{60} (90 mg, 0.12 mmol, 4 equiv.) and N-methylglycine (11 mg, 0.12 mmol, 4 equiv.) under reflux in toluene. The residue was purified by using gel permeation chromatography on BioBeads SX-1 eluting with dichloromethane. Further purification was by column chromatography (SiO_2) using dichloromethane as eluent. The final product was dried under reduced pressure for 24 h. (Yield: 25 mg, 30%). UV/Vis (CH_2Cl_2): λ_{max} (ε, M^{-1} cm^{-1}) = 256 (170600), 422 (557700), 516 (120000), 544 (120100) nm. ^{1}H NMR (300 MHz, $CDCl_3$): δ 8.78-8.93 (m, 10H), 8.30-8.38 (m, 1H), 7.89-8.08 (m, 11H), 7.50-7.70 (m, 11H), 7.30-7.33 (m, 1H), 6.59-7.21 (m, 8H), 4.93 (s, 1H), 4.83 (d, J = 9.5 Hz, 1H), 3.94-4.17 (m, 3H), 3.49-3.70 (m, 2H), 3.20 (s, 3H), 2.70 (s, 12H), 1.97-2.14 (m, 2H), 1.27-1.53 (m, 72H) ppm; ^{13}C NMR (76 MHz, $CDCl_3$): δ ppm; FT-IR(ATR): ν = 3412.2 (w), 2951.0 (m), 2919.1 (m), 2861.0 (w), 1722.8 (w), 1590.3 (s), 1487.2 (m), 1452.6 (m), 1387.1 (w), 1359.1 (m), 1324.3 (w), 1299.0 (w), 1253.8 (w), 1204.7 (w), 1175.9 (w), 1107.2 (w), 1087.6 (w), 1059.7 (w), 1026.7 (s), 997.7 (s), 942.5 (w), 929.6 (w), 885.6 (w), 839.3 (w), 796.9 (s), 744.9 (w), 721.5 (w), 627.9 (m), 598.9 (w), 574.8 (w), 553.5 (w), 526.3 (s), 478.4 (w) cm^{-1}; MALDI-TOF-MS (dithranol): m/z = 2672 ([M - H]$^+$); HRMS (ESI-MS); calc'd for $[C_{189}H_{136}O_5N_9Zn]^+$ = 2674.995, found: 2674.9968.

Femtosecond transient absorption (fs-TA) spectroscopy. Fs-TA spectroscopy experiments were performed using an Ultrafast Femtosecond Laser Source (Libra) by Coherent incorporating a diode-pumped, mode locked Ti:Sapphire laser (Vitesse) and diode-pumped intra-cavity doubled Nd:YLF laser (Evolution) to generate a compressed laser output of 1.45 W. For optical detection, a Helios transient absorption spectrometer (3 ns delay line) coupled with femtosecond harmonics generator both provided by Ultrafast Systems LLC was used. The source for the pump and probe pulses were derived from the fundamental output of Libra (Compressed output 1.45 W, pulse width 100 fs) at a repetition rate of 1 kHz. 95% of the fundamental output of the laser was introduced into a TOPAS-Prime-OPA system with 290-2600 nm tuning range from Altos Photonics Inc., (Bozeman, MT), while the remaining output was used for generation of white light continuum. Kinetic traces at appropriate wavelengths were assembled from the time-resolved spectral data. Data analysis including generation of decay associated spectra was performed using Surface Xplorer software supplied by Ultrafast Systems. All measurements were conducted in degassed solutions at 298 K. The estimated error in the reported rate constants is $\pm$10%.

Conflicts of interest

There are no conflicts to declare.

Acknowledgements

This material is based upon work supported by the National Science Foundation under grant number 2000988 to FD. This work was also partly supported by World Premier International Research Center Initiative (WPI Initiative), MEXT, Japan, JSPS KAKENHI Grant No. JP16H06518 (Coordination asymmetry), and CREST JST, Japan (Grant No. JPMJCR1665). The computatonal work was completed utilizing the Holland Computing Center of the University of Nebraska, which receives support from the Nebraska Research Initiative.

Notes and references

1 (a) L. R. Milgrom, *The Colors of Life,* Oxford University Press, 1997. (b) J. P. Hill, F. D'Souza and K. Ariga 'Porphyrinoids: Highly Colored, Redox Active Scaffolds for Supramolecular Synthesis' in *Supramolecular Chemistry: From Molecules to Nanomaterials* Eds. P. A. Gale and J. W. Steed, John Wiley & Sons Ltd, Chichester, UK, 2012, pp 1713-1730.

2 *The Porphyrin Handbook* K. M. Kadish, K. M. Smith and R. Guilard, Eds.; Academic Press: Burlington, MA**,** 2000.

3 (a) N. Nelson and C. F. Yocum, *Ann. Rev. Plant Biol.*, 2006, **57**, 521; (b) G. Renger, *Biochim. Biophys. Acta,* 2012, **1817**, 1164.

4 D. Gust, T. A. Moore and A. L. Moore in *Electron Transfer in Chemistry*, ed. V. Balzani, Wiley, Weinheim, 2001, Vol. 3, pp 272–336.

5 A. G. Coutsolelos, L. Ladomenou, G. Charalambidis and D. Daphnomili in *Handbook of Porphyrin Science*, eds. K. M. Kadish, K. M. Smith, R. Guilard, World Scientific, Singapore, 2014, Vol. 34, pp 239–320.

6 (a) S. Shoji and H. Tamiaki, *Dyes and Pigments*, 2019, **160**, 514; (b) C. Chappaz-Gillot, P. L. Marek, B. J. Blaive, G. Canard, J. Burck, G. Garab, H. Hahn, T. Javorfi, L. Kelemen, R. Krupke, D. Mossinger, P. Ormos, C. M. Reddy, C. Roussel, G. Steinbach, M. Szabo,; A. S. Ulrich, N. Vanthuyne, A. Vijayaraghavan, A. Zupcanova and T. S. Balaban, *J. Am. Chem. Soc.*, 2012, **134**, 944.

7 D. Gust and T. A. Moore in *The Porphyrin Handbook*, eds. K. M. Kadish, K. M. Smith and R. Guilard, Academic Press: Burlington, MA**,** 2000, Vol**.** 8, pp. 153–190.

8 R. Ziessel, G. Ulrich, A. Haefele and A. Harriman, *J. Am. Chem. Soc.*, 2013, **135**, 11330.

9 Y. Jiang and J. MacNeill, *Chem. Rev.*, 2017, **117**, 838.

10 G. Charalambidis, E. Georgilis, M. K. Panda, C. E. Anson, A. K. Powell, S. Doyle, D. Moss, T. Jochum, P. N. Horton, S. J. Coles, M. Linares, D. Beljonne, J.-V. Naubron, J. Conradt, H. Kalt, A. Mitraki, A. G. Coutsolelos and T. S. Balaban, *Nat. Commun.*, 2016, **7**, 12657.

11 (a) S. Fukuzumi and K. Ohkubo, *Coord. Chem. Rev*. 2010, **254**, 373. (b) C. F. Yocum, *Coord. Chem. Rev*., 2007, **252**, 296; (c) J. P. McEvoy and G. W. Brudvig, *Chem. Rev*., 2006, **106**, 4455; (d) L. M. Utsching and M. C. Thurnauer, *Acc. Chem. Res*., 2004, **37**, 439.

12 For example: (a) S. Fukuzumi, K. Saito, K. Ohkubo, T. Khoury, Y. Kashiwagi, M. A. Absalom, S. Gadde, F. D'Souza, Y. Araki, O. Ito and M. J. Crossley, *Chem. Commun.*, 2011, **47**, 7980; (b) S. Fukuzumi, K. Ohkubo, F. D'Souza and J. L. Sessler, *Chem. Commun*., 2012, **48**, 9801; (c) J. Otsuki, *J. Mater. Chem. A*, 2018, **6**, 6710.

13 For example: (a) S. D. Straight, G. Kodis, Y. Terazono, M. Hambourger, T. A. Moore, A. L. Moore and D. Gust, *Nat. Nanotech.*, 2008, **3**, 280. (b) W. Maes, J. Vanderhaeghen, S. Smeets, C. V. Asokan, L. M. Van Renterghem, F. E. Du Prez, M. Smet and W. Dehaen, *J. Org. Chem.*, 2006, **71**, 2987.

14 (a) F. D'Souza, N. K. Subbaiyan, Y. Xie, J. P. Hill, K. Ariga, K. Ohkubo and S. Fukuzumi, *J. Am. Chem. Soc.*, 2009, **131**, 16138; (b) F. D'Souza, A. L. Schumacher, J. P. Hill, P. A. Karr, M. E. Zandler, Y. Xie, K. Ariga, A. S. D. Sandanayaka, Y. Araki and O. Ito, *Electrochem. Soc. Trans.*, 2008, **13**, 127; (c) A. L. Schumacher, A. S. D. Sandanayaka, J. P. Hill, K. Ariga, P. A. Karr, Y. Araki, O. Ito and F. D'Souza, *Chem. Eur. J.*, 2007, **13**, 4628; (d) J. P. Hill, A. S. D. Sandanayaka, A. L. McCarty, P. A. Karr, M. E. Zandler, R. Charvet, K. Ariga, Y. Araki, O. Ito and F. D'Souza, *Eur. J. Org. Chem.,* 2006, **2006**, 595.

15 (a) W. A. Webre, H. B. Gobeze, S. Shao, P. A. Karr, K. Ariga, J. P. Hill and Francis D'Souza, *Chem. Commun.,* 2018, **54**, 1351; (b) J. P. Hill, M. E. El-Khouly, R. Charvet, N. K. Subbaiyan, K. Ariga, S. Fukuzumi and F. D'Souza, *Chem. Commun.*, 2010, **46**, 7933; (c) Y. Xie, J. P. Hill, A. L. Schumacher, A. S. D. Sandanayaka, Y. Araki, P. A. Karr, J. Labuta, F. D'Souza, O. Ito, C. E. Anson, A. K. Powell and K. Ariga, *J. Phys. Chem. C*, 2008, **112**, 10559.

16 (a) M. K. Chahal, J. Labuta, V. Březina, P. A. Karr, Y. Matsushita, W. A. Webre, D. T. Payne, K. Ariga, F. D'Souza and J. P. Hill, *Dalton Trans.*, 2019, **48**, 15583; (b) M. K. Chahal, D. T. Payne, Y. Matsushita, J. Labuta, K. Ariga and J. P. Hill, *Eur. J. Org. Chem.*, 2020, **2020**, 82.

17 (a) M. R. Wasielewski, *Acc. Chem. Res*., 2009, **42**, 1910; (b) F. D'Souza and O. Ito, *Coord. Chem. Rev*., 2005, **249**, 1410.

18 (a) H. Imahori, T. Umeyama and S. Ito, *Acc. Chem. Res*., 2009, **42**, 1809; (b) T. M. Figueira-Duarte, A. Gegout and J.-F. Nierengarten, *Chem. Commun*. 2007, 109; (c) S. Fukuzumi, S. *Phys. Chem. Chem. Phys.,* 2008, **10**, 2283, (d) V. Sgobba and D. M. Guldi, *Chem. Soc. Rev*., 2009, **38**, 165.

19 (a) L. R. Milgrom, *Tetrahedron*, 1983, **39***,* 3895; (b) J. P. Hill, I. J. Hewitt, C. E. Anson, Annie K. Powell, A. L. McCarthy, P. Karr, M. Zandler and F. D'Souza, *J. Org. Chem.*, 2004, **69**, 5861. (c) J. P. Hill, W. Schmitt, A. L. McCarty, K. Ariga and F. D'Souza, *Eur. J. Org. Chem.*, 2005, **2005**, 2893.

20 (a) M. Maggini, G. Scorrano and M. Prato, *J. Am. Chem. Soc*., 1993, **115**, 9798. (b) V. Garg, G. Kodis, M. Chachisvilis, M. Hambourger, A. L. Moore, T. A. Moore and D. Gust, *J. Am. Chem. Soc.*, 2011, **133,** 2944.

21 *Principles of Fluorescence Spectroscopy*, 3rd Ed., Ed.: J. R. Lakowicz, Springer, Singapore, 2006.

22 M. J. Frisch, G.W. Trucks, H. B. Schlegel, G. E. Scuseria, M. A. Robb, J. R. Cheeseman, V. G. Zakrzewski, J. A. Montgomery, R. E. Stratmann, J. C. Burant, S. Dapprich, J. M. Millam, A. D. Daniels, K. N. Kudin, M. C. Strain, O. Farkas, J. Tomasi, V. Barone, M. Cossi, R. Cammi, B. Mennucci, C. Pomelli, C. Adamo, S. Clifford, J. Ochterski, G. A. Petersson, P. Y. Ayala, Q. Cui, K. Morokuma, D. K. Malick, A. D. Rabuck, K. Raghavachari, J. B. Foresman, J. Cioslowski, J. V. Ortiz, B. B. Stefanov, G. Liu, A. Liashenko, P. Piskorz, I. Komaromi, R. Gomperts, R. L. Martin, D. J. Fox, T. Keith, M. A. Al-Laham, C. Y. Peng, A. Nanayakkara, C. Gonzalez, M. Challacombe, P. M. W. Gill, B. G. Johnson, W. Chen, M. W. Wong, J. L. Andres, M. Head-Gordon, E. S. Replogle and J. A. Pople, *Gaussian 16*, Revision A.03, Gaussian, Inc., Wallingford CT, 2016.

23 D. Rehm and A. Weller, *Isr. J. Chem*. 1970, **8,** 259.

24 Gibbs free-energy change associated for excited state charge separation (CS) and dark charge recombination (CR) were estimated according to equations (i-iii):

$$-\Delta G_{CR} = E_{ox} - E_{red} + \Delta G_S \qquad \text{(i)}$$

$$-\Delta G_{CS} = \Delta E_{00} - (-\Delta G_{CR}) \qquad \text{(ii)}$$

where ΔE_{00} corresponds to the singlet energy of the sensitizer (mid-point energy of 0,0 absorption and emission peaks). The term ΔG_S refers to electrostatic energy calculated according to dielectric continuum model (see equation iii). The E_{ox} and E_{red} represent the oxidation potential of the electron donor and the first reduction potential of the electron acceptor, respectively.

$$\Delta G_S = e^2 / 4\,\pi\,\varepsilon_o\,[\,-\,1/R_{cc}\,\varepsilon_R) \qquad \text{(iii)}$$

The symbols ε_0 and ε_R represent vacuum permittivity and dielectric constant of 1,2-dichlorobenzene used for photochemical and electrochemical studies (= 8.93). R_{CC} are the center-to-center distance between donor and acceptor entities from the computed structures in Figure 4.

25 H. Imahori, K. Tamaki, D. M. Guldi, C. Luo, M. Fujitsuka, O. Ito, Y. Sakata and S. Fukuzumi, *J. Am. Chem. Soc*. 2001, **123**, 2607.

26 F. D'Souza and O. Ito, *Sci, Progress*, 2013, **96**, 369.

27 D. M. Guldi and P. V. Kamat in Fullerenes Eds., K. M. Kadish and R. S. Ruoff, Wiley, New York, 2000, chapter 5, pp 225-281.

28 M. E. El-Khouly, C. A. Wijesinghe, V. N. Nesterov, M. E. Zandler, S. Fukuzumi and F. D'Souza, *Chem. Eur. J.* 2012, **18**, 13844.

29 S. Punidha, J. Sinha, A. Kumar and M. Ravikanth, *J. Org. Chem.*, 2008, **73**, 323.